ASDJ
AINSHAMS DENTAL JOURNAL

Print ISSN 1110-7642
Online ISSN 2735-5039

AIN SHAMS DENTAL JOURNAL
Official Publication of Ain Shams Dental School
September 2024 • Vol. 35

Possible Modulatory Role of Quercetin Flavonoid on Monosodium Glutamate-Induced Chronic Toxicity in Parotid Glands of Albino Rats (Histologic and ultrastructural study)

Rania Awad[1], Omnia Khaled[2], Iman Fathy[1]

Aim: Monosodium glutamate (MSG) is a universal flavoring booster utilized in the food industry as an additive. This research investigates whether MSG has any effect on the histological and ultrastructural features of the parotid gland of rats and the potential modulatory effects of a famous antioxidant flavonoid Quercetin (QN).
Materials and Methods: 24 male albino rats were divided evenly into 3 groups. Group 1 (control group) received orally the vehicle Dimethyl sulfoxide daily (DMSO) for 8 weeks. Group II (MSG group): received a daily dose of MSG (30mg/Kg. b. w.) dissolved in 0.5 ml distilled water through oral gavage for 8 weeks Group III (MSG + QN) received orally monosodium glutamate (30mg/kg. b. w.) dissolved in 0.5 ml distilled water through oral gavage followed by quercetin (10 mg/kg. body weight) in (DMSO) daily for 8 weeks concomitantly. Parotid glands were dissected and assessed histologically by H&E staining and ultra-structurally by Transmission electron microscopy.
Results: MSG group evidenced loss of normal glandular configuration, most of the acini had vacuolated cytoplasm. Nuclear pleomorphism and hyperchromatism, distorted ducts, congested dilated blood vessels and connective tissue heavily infiltrated with inflammatory cells were observed. MSG+QN group exhibited significant amelioration in histological and ultrastructural assessment.
Conclusion: Administration of quercetin has protective effects against toxicity caused by chronic MSG intake on parotid glands of rats.

Keywords: Parotid gland, Monosodium glutamate, Quercetin, oxidative stress, antioxidant.

---

1. Associate professor of oral biology, Faculty of dentistry Ain Shams university, Cairo, Egypt.
2. Demonstrator of oral biology, Faculty of dentistry Ain Shams university, Cairo, Egypt.
Corresponding author: Omnia khaled, email: omnia.Abdelrahman@dent.asu.edu.eg

Introduction

One of today's most significant issues is the investigation of the mechanisms that underlie the effects of numerous food additives on human and animal species. Monosodium glutamate (MSG) or E621, with chemical composition of ($C_5H_8NO_4Na$), is the sodium salt of L-glutamic acid that is consumed worldwide as a flavor booster. It exhibits an umami taste that enhances the juicy taste of food, resembling the natural glutamates in food.[1]

Due to its flavor-boosting qualities, E621 is applied as a food additive in the form of hydrolyzed protein or as purified monosodium salt. It is an odorless, crystalline white powder with a melting point of 232 ° C and a molecular mass of 169. 11 g/mol.[2] It has been found in preserved dinners, processed meats like luncheon, hot dogs, and sausages, potato chips, canned tuna, soups, sauces such as ketchup, mayonnaise, mustard, barbecue, soy sauce, salad dressings, and several varieties of cheese (Roquefort, Parmesan, and so on).[3]

MSG has been proven to induce an imbalance between free oxygen radicals and antioxidants by producing oxygen-derived free radicals and related reactive oxygen species (ROS), which are harmful to biological systems because they react with DNA, proteins, and lipids, causing cellular damage.[4] It has also shown to increase levels of interleukin-6 and tumor necrosis factor-alpha-mediated inflammatory response as well as hindering the activity of the antioxidant enzymes such as superoxide dismutase (SOD) and glutathione metabolizing enzymes like glutathione reductase and glutathione peroxidase.[5,6]

Quercetin (3, 3', 4', 5, 7-pentahydroxyflavone), a well-recognized antioxidant agent, is one of the most significant bioflavonoids found in over 20 different plants including Morus alba, Moringa oleifera, Hypericum perforatum, Lactuca sativa, and C. spinosa.[7] Quercetin has recently been used as a dietary supplement and may be effective in improving many diseases. Some of the beneficial effects include cardiovascular protection, anticancer, antidiabetic, antitumor, anti-allergic, anti-ulcer, antiviral, anti-inflammatory activity, antihypertensive, gastroprotective effects, immunomodulatory, and anti-infective.[8–12]

The antioxidant properties of quercetin have been the subject of extensive research in recent years. These studies have focused on the effects of quercetin on glutathione (GSH) levels, enzymatic activity such as superoxide dismutase (SOD), signal transduction pathways, and reactive oxygen species (ROS) caused by environmental and toxicological factors.[13] Quercetin (QN) exhibits a significant antioxidant action by sustaining oxidative balanced environment.[10]

Based on the above-mentioned data, we decided to study the effects of oxidative stress produced by MSG on the parotid glands of rats from a histologic and ultrastructural view while assessing the ameliorating effect of a strong antioxidant like quercetin.

Materials and Methods

Materials:

Chemicals and Treatments

- Mono-sodium glutamate (E621) with a purity of 99% was purchased from Hulunbeier Northeast Fufeng Biotechnologies Co. (China) as a white powder that dissolves in water.
- Quercetin hydrate was purchased from Nano Gate laboratory (Egypt) in the form of yellow powder with 95% purity.

Animals

24 male albino rats weighing between 150-200 grams were settled in the Ain Shams Medical Research Center, Faculty of Medicine, Ain Shams University, Egypt, under balanced temperature and a 12-hour

dark-light cycle, five animals per cage. Animals were fed a standard diet of rat chow and tap water, as reviewed and approved by institution guidelines of Ain-Shams university ethical committee. Approval number (FDASU-Rec IM122111).

Experimental Design

After acclimating the animals for a week, they were split into three groups.

Group I (Control) : in which 8 rats received, by oral gavage, the vehicle 1% Dimethyl sulfoxide solution daily (DMSO) for 8 weeks.[11]

Group II (MSG group) : in which 8 rats were given a daily dose of MSG (30 mg/kg. b. w.) dissolved in 0. 5 ml of distilled water by oral gavage for 8 weeks.[14]

Group III **:** (MSG + QN group) : in which 8 rats received orally monosodium glutamate (30 mg/kg. b. w.) dissolved in 0. 5 ml of distilled water through oral gavage, followed by quercetin (10 mg/kg. b. w.) in a 1% (DMSO) solution daily for 8 weeks (coadministration). [15,16]

At the end of the experimental period (8 weeks), all rats were sacrificed by a high dose of anesthesia, and the parotid glands (PG) on both sides were excised. The right side was assigned for histological inspection by a light microscope, and the left side was assigned for transmission electron microscope (TEM).

Histopathological Examination

Right side parotid glands' histological analysis was performed after specimens were fixed in a 10% formaldehyde solution for 24 hours and then stained with Hematoxylin and Eosin (H&E).[17]

Histomorphometric Analysis

This study was done using computerized image analyzer (Fiji Image J processing package software (https ://fiji. sc/)) and saved as TIFF. The resulting images were analyzed using Video Test Morphology software (VideoTesT, St Petersburg, Russia) with a specific built-in routine for calibrating distance measurement and stain quantification. This was done in order to assess the mean acinar diameter and the percentage of vacuolation of the cytoplasm of acinar cells. Five parotid H&E sections were selected from each group, and five fields were analyzed for mean acinar diameter and percentage of cytoplasmic vacuolation of acinar cells in a morphometric study under LM at 400 magnification.[18]

Statistical Analysis

The data was run through SPSS for statistical analysis. The normality hypothesis of all continuous variables was tested using the Shapiro-Wilk test of normality. The statistical significance of each parameter within the studied groups was determined using the analysis of variance (ANOVA) test. P-values $\leq$ 0. 05 were considered statistically significant. Also, Tukey Kramer Post Hoc test was used to define the significance between each two groups.

Transmission Electron Microscope Examination:

Specimens were fixed for 1 hour in buffered glutaraldehyde (2. 5%), followed by 2 hours in osmium tetroxide (1%). Immersion in ethanol of increasing concentrations was then done for the dehydration of specimens. Specimens were then positioned in propylene oxide, and then resin epon 812 was used for embedding. Samples were cut into semithin sections and stained with toluidine blue, then ultrathin sections (60 nm) were contrasted with 4% uranyl acetate and Reynold's lead citrate.[19] They were then inspected and photographed using a transmission electron microscope (TEM) SEOTEM-100 (SUMY Electron Optics – Ukraine) in the Electron Microscopy unit in the Geology Department, Faculty of Sciences, Ain Shams University.

Results

H&E Results:

Group I (Control)

The results of this group revealed a normal parenchymal architecture of the parotid gland, which consists of secretory end pieces and collecting ducts. The secretory end piece consisted of spherical acini composed of serous cells, each containing basal rounded deeply basophilic nuclei. Intercalated ducts (ID) were composed of cuboidal cells surrounding a narrow lumen, while the striated ducts (SD) were highly eosinophilic and consisted of low columnar cells with centrally located nuclei (Fig. 1a).

The excretory ducts (ED) were lined by pseudostratified columnar epithelium with goblet cells. They showed a relatively wide lumen and were surrounded by fibrous connective tissue septa with apparently normal blood vessels (BVs) (Fig. 1b).

Group II (MSG)

This group expressed loss of normal glandular framework. Most acini displayed atypical morphology with indistinct boundaries. The majority of the acini had vacuolated cytoplasm. Nuclear pleomorphism and hyperchromatism, along with an increased nuclear cytoplasmic ratio, were clearly visible. Additionally, there were some giant nuclei (Fig. 1c). The ductal system showed a bizarre outline and appeared dilated, where striated ducts (SD) showed vacuolations while excretory ducts (ED) showed a flattened outline with distorted cells and loss of psudostratified pattern. BVs appeared engorged with RBCs, and inflammatory cells heavily infiltrated the connective tissue (CT) around the excretory duct (Fig. 1 c-d).

Group III (MSG+QN)

Most acini appeared spherical in shape with basophilic cytoplasm and showed significant decrease in cytoplasmic vacuolation compared to the MSG group. However, some acini showed hyperchromatic, pleomorphic nuclei and variable-sized cytoplasmic vacuoles. Most of the ductal elements regained their normal configuration, normal connective tissue, and blood vessels were less dilated and congested. Coadministration of MSG & QN resulted in apparent decrease in the damage of PG which was specially evident in ductal elements and vasculature. (Fig. 1 e-f)

TEM Results

Group I (Control)

Ultrastructural examination of this group revealed acini composed of pyramidal cells with round nuclei located at the base. These nuclei exhibited prominent nucleoli and peripheral chromatin condensation. The nuclei were surrounded by parallel arrays of rough endoplasmic reticulum (RER) at the basal and lateral regions. Apical secretory granules, homogeneous in density, were evident (Fig. 2a-c). The SD cells were columnar with central round nuclei and a regular lumen. The basal portion showed deep infoldings in which a large number of mitochondria were radially arranged. The ducts were associated with blood vessels (Fig. 2d). The ID lined by simple cuboidal cells with large round nuclei (Fig. 2e). The ED was lined by pseudostratified epithelium with large round nuclei at different levels (Fig. 2f).

Group II (MSG)

MSG group showed significant atrophy, with irregular acinar and cellular boundaries. Some nuclei were pyknotic with irregular membrane indentations, while some acinar cells showed nuclear division without cytoplasmic division. Intracellular cytoplasmic vacuolation and other signs of cellular degeneration were present, along with intercellular spaces. The RER was dilated and fragmented, and the mitochondria had hazy appearances with their cristae becoming less distinct. Large irregular membrane-bound granules of varying densities and sizes, formed from the accumulation of smaller granules, were observed. Desmosomal attachments were also significantly less apparent, resulting in widened intercellular junctions (Fig. 3a-b).

SD showed a disrupted outline with stagnant secretion. Swollen mitochondria with indistinct basal infoldings were observed, along with cytoplasmic vacuoles. Some of the nuclei appeared pyknotic with irregular nuclear membranes (Fig. 3c). ID showed an ill-defined outline of cells and cellular boundaries with abnormal cellular junctions, giant nuclei with clumped chromatin (Fig. 3d). ED cells revealed extensive vacuolations with abnormal cellular junctions (Fig. 3e). There were dilated and congested BVs, extravasated blood, and an abnormal number of inflammatory cells (Fig. 3e-f).

Group III (MSG+QN)

Specimens showed pyramidal acinar cells with prominent cellular borders, some of them still had irregular nuclear membranes. Abundant, well-formed RER strands were apparent alongside normal mitochondria. Few slightly hazy mitochondria were also observed. Normal secretory granules and partial restoration of junctional complexes were evident. Cells displayed relatively fewer intracytoplasmic vacuolations (Fig. 4 a-c). SD manifested relatively fewer swollen mitochondria, distinct basal infoldings, and a normal nuclear outline (Fig. 4d). ID showed a normal outline and cellular junctions with a regular lumen. Intercellular edema was observed (Fig. 4e). ED had basal and columnar cells with fewer vacuolations and normal microvilli (Fig. 4f).

Statistical Results

Acini Diameter

The MSG group had the smallest mean diameter, while the control group had the greatest mean diameter. The results of a test using the analysis of variance (ANOVA) method showed that there was a statistically significant gap between all groups. (P<0. 0001). Tukey's post hoc revealed significant difference between each two groups (Table 1) (Fig. 5).

Area Percent of Vacuolization

The group with the highest recorded mean area percentage was the MSG group, while the control group had the lowest recorded value. The results of a test using the analysis of variance (ANOVA) method showed that there was a statistically significant difference among all groups. (P < 0. 0001) Tukey's post hoc revealed significant difference between each two groups (Table 1) (Fig. 5).

Table 1: Morphometric analysis for all groups and significance of the difference using (ANOVA) test.

P. O. C	Control		MSG		MSG+QN	
	Area percent of vacuolization	Acinar diameter	Area percent of vacuolization	Acinar diameter	Area percent of vacuolization	Acinar diameter
Mean	1. 4[a]	121. 94[a]	13. 62[c]	58. 91[c]	3. 25[b]	99. 1[b]
Std Dev	0. 71	17. 96	2. 09	8. 2	1. 15	7
Std error	0. 32	7. 33	0. 93	3. 35	0. 52	2. 84
Max	2. 43	152. 2	02 .17	45 .71	4. 52	107
Min	0. 46	105	11. 56	46. 2	73 .1	3 .90
F-value	Acinar diameter	41. 771				
	Area percent of vacuolization	105. 045				
P-value	< 0. 0001*					

*significant at p<0.05 Tukey's post hoc test: means sharing the same superscript letter are not significantly different.

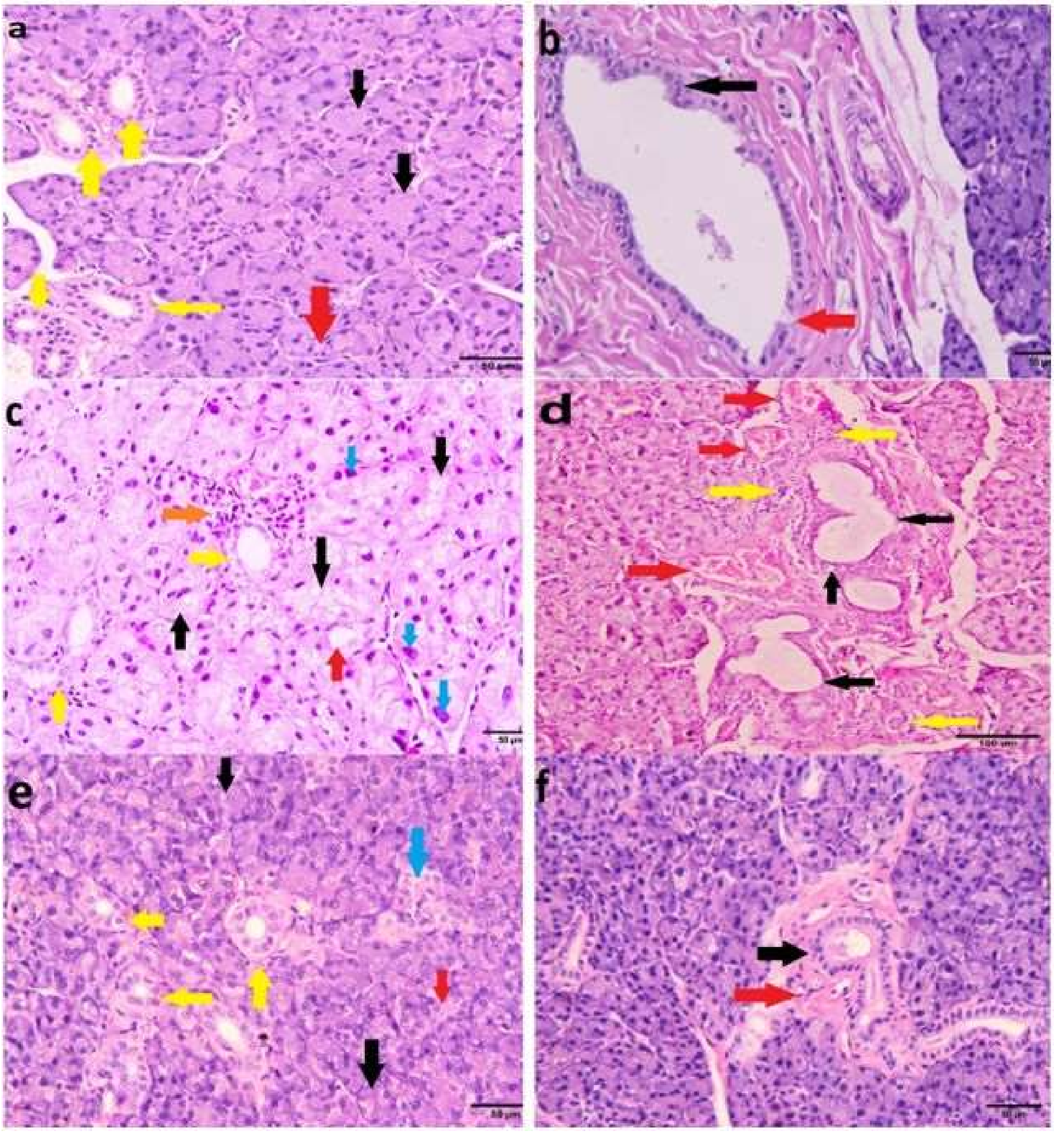

Figure 1: Photomicrograph of rats parotid gland: **(a, b) Group I; (a)** basophilic serous acini of normal outline with basal round nuclei (black arrows), ID lined by cuboidal cells (red arrows), SD lined by eosinophilic columnar cells (yellow arrows) (H&E x400), **(b)** ED lined by pseudostratified epithelium (black arrow) with goblet cells (red arrow) surrounded by fibrous C.T(H&E x400), **(c, d) Group II; (c)** disturbed architecture of acini with extensive vacuolation (black arrows) and large hyperchromatic nuclei (blue arrows), ID with abnormal outline (red arrow), SD with vacuolation (yellow arrows), infl. Cells infiltration (orange arrow) (H&E x400), **(d)** ED with flattened outline & distorted cells with loss of pseudostratified pattern (black arrows) surrounded by heavy infiltration of infl. Cells (yellow arrows) and dilated congested blood vessels (red arrows)(H&E x200), **(e, f) Group III; (e)** basophilic acini with apparently restored outline & relatively less cytoplasmic vacuolations (black arrows), ID with restored outline (red arrow), some SD restored their outline (yellow arrows) other SD with disturbed architecture (blue arrow) (H&E x400), **(f)** ED restored its pseudostratified appearance (black arrow) surrounded by fibrous C.T with less infl. Cells infiltration (red arrows) (H&E x400).

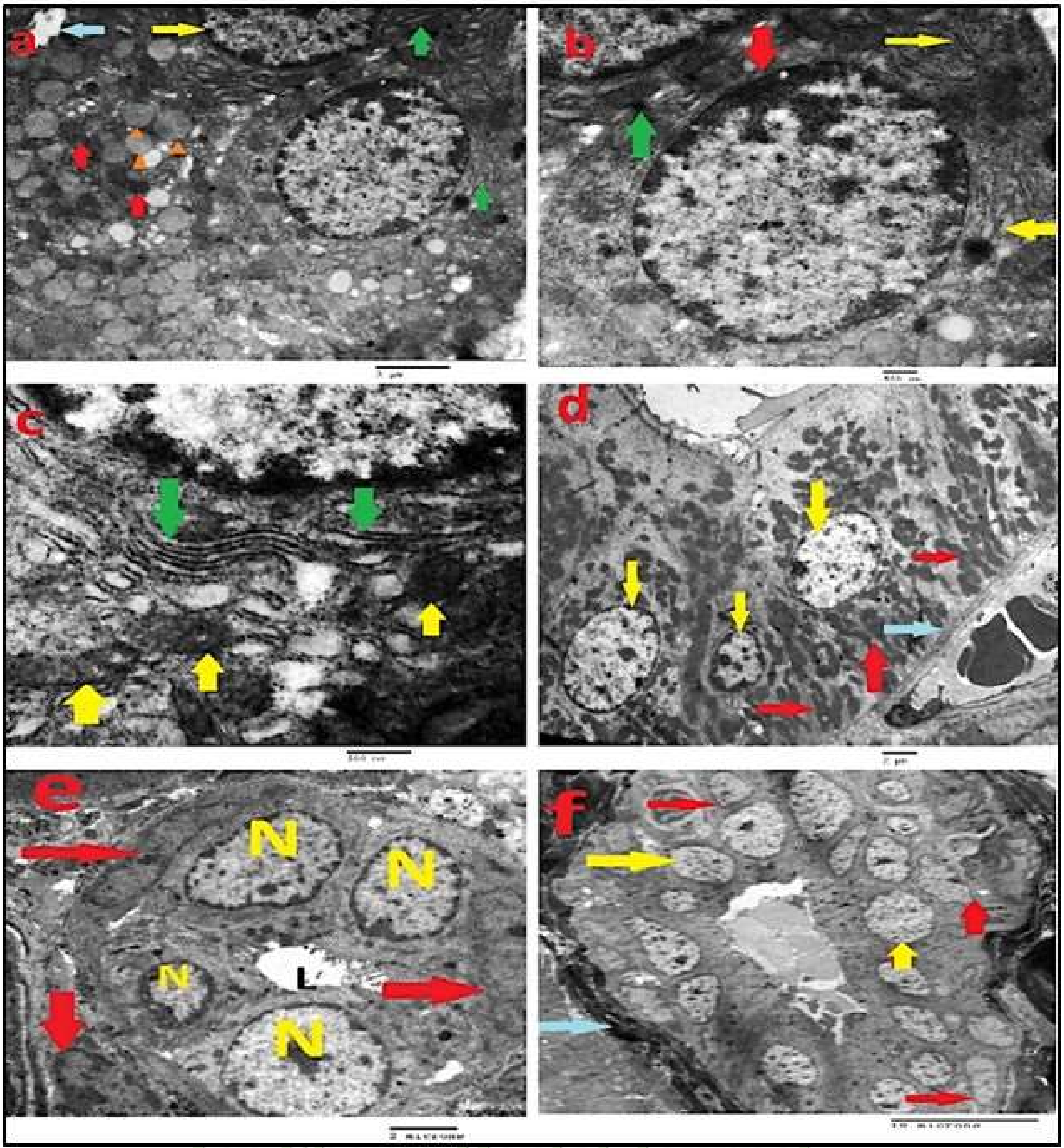

Figure 2: Electron micrographs of control group showing: acinar cells **(a-c)**, **(a)** pyramidal acinar cells with basal round nuclei (yellow arrow), parallel arrays of RER (green arrows), homogenous secretory granules (orange arrows) and narrow acinar lumen (blue arrow), **(b)** regular and well-defined binuclear membrane (red arrow), parallel arrays of RER basal and lateral to the nucleus (yellow arrows), desmosomal junction (green arrow). **(c)** RER studded with ribosomes (green arrows), numerous mitochondria with internal cristae (yellow arrows), **[Uranyl acetate and lead citrate (a) x2000, (b) x4000, (c) x7500]. (d)** striated duct lined with columnar cells with central round nuclei (yellow arrows), deep basal infoldings between which numerous mitochondria are radially packed (red arrows), note the adjacent blood vessel (blue arrow) **[Uranyl acetate and lead citrate x1000]**, **(e)** ID lined by cuboidal cells with central large round nuclei (N) and narrow lumen (L) , note the myoepithelial cells (red arrows), **[Uranyl acetate and lead citrate x2000]**. **(f)** ED lined by pseudostratified epithelium with large round nuclei at different levels basal cells (red arrows) & columnar cells (yellow arrows) surrounded by connective tissue (blue arrow) **[Uranyl acetate and lead citrate x2500].**

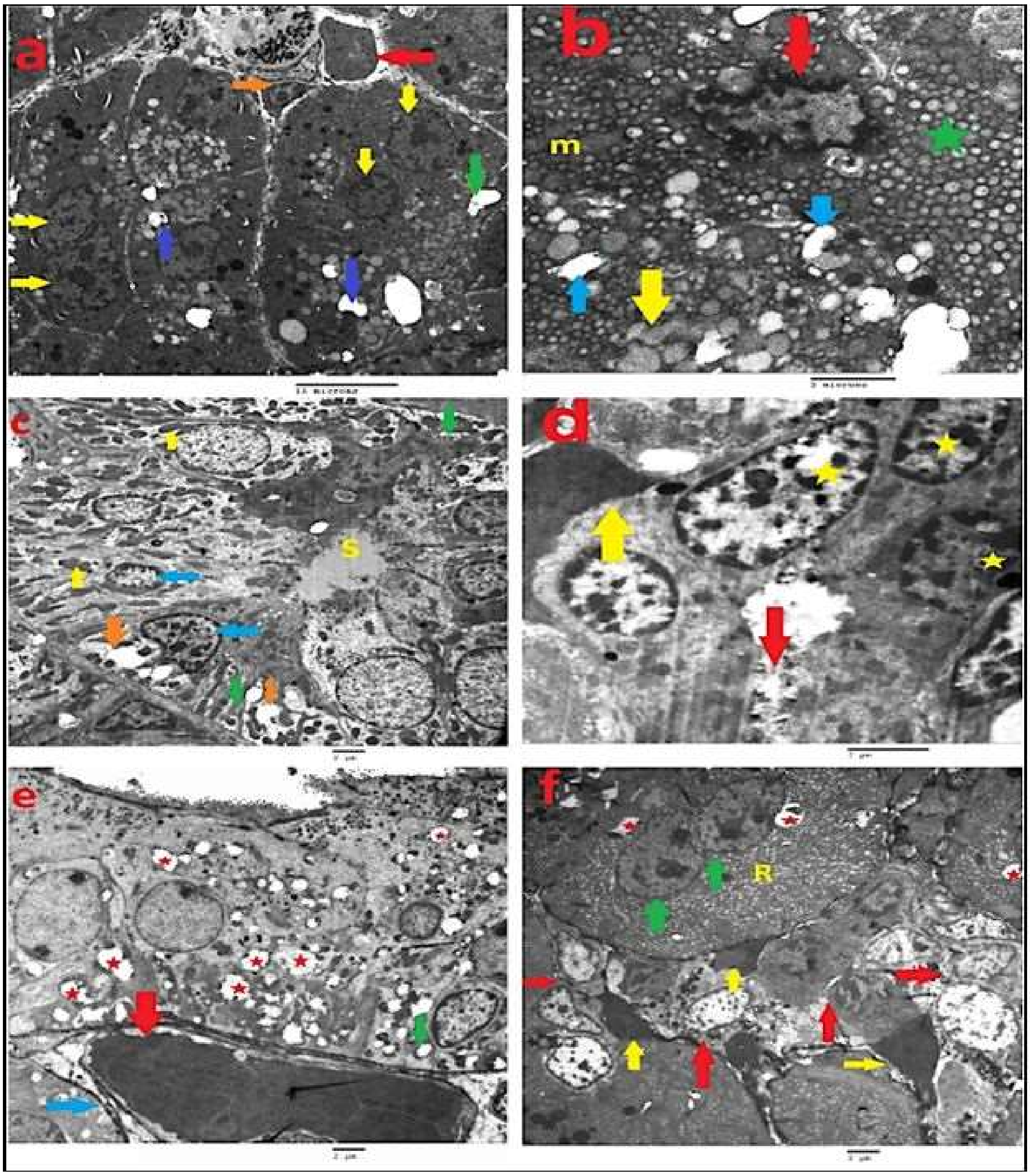

Figure 3: Electron micrograph of MSG group showing: **(a)** shrunken & atrophied acini with disturbed architecture, numerous intercellular (green arrows) and intracellular (blue arrows) vacuoles. Acinar cells showed division of nucleus without division of cytoplasm (yellow arrows), note the extravasated blood (red arrow) and inflammatory cells (orange arrow), **(b)** acinar cell with pyknotic nucleus & irregular nuclear indentations (red arrow). Dilated & fragmented RER (star). Ill-defined mitochondria with blurred cristae (m), cytoplasmic vacuolations (blue arrows), fused irregular membrane-bound secretory granules (yellow arrow). **(c)** SD showing disrupted outline with stagnant secretion (S), swollen mitochondria (yellow arrows) with indistinct basal infoldings (green arrows), cytoplasmic vacuoles (orange arrows), pyknotic and irregular nuclei (blue arrows), **(d)** ID showing ill-defined outline of cells and cellular boundaries with abnormal cellular junctions (red arrow), giant nuclei with clumped chromatin (star), congested BV (yellow arrow), **(e)** ED showing numerous cytoplasmic vacuolations (star), disrupted cellular junctions (green arrows), dilated and congested BV (red arrow) with abnormal endothelial cell (blue arrow). **(f)** Heavy infiltration of infl. cells (red arrows) with extravasated blood between the acini (yellow arrows) binucleated acinar cell (green arrow) with dilated RER (R), vacuoles (stars). **[Uranyl acetate and lead citrate (a) x2500, (b) x10000, (c) x1000, (d) x2500, (e) x1000, (f) x1000].**

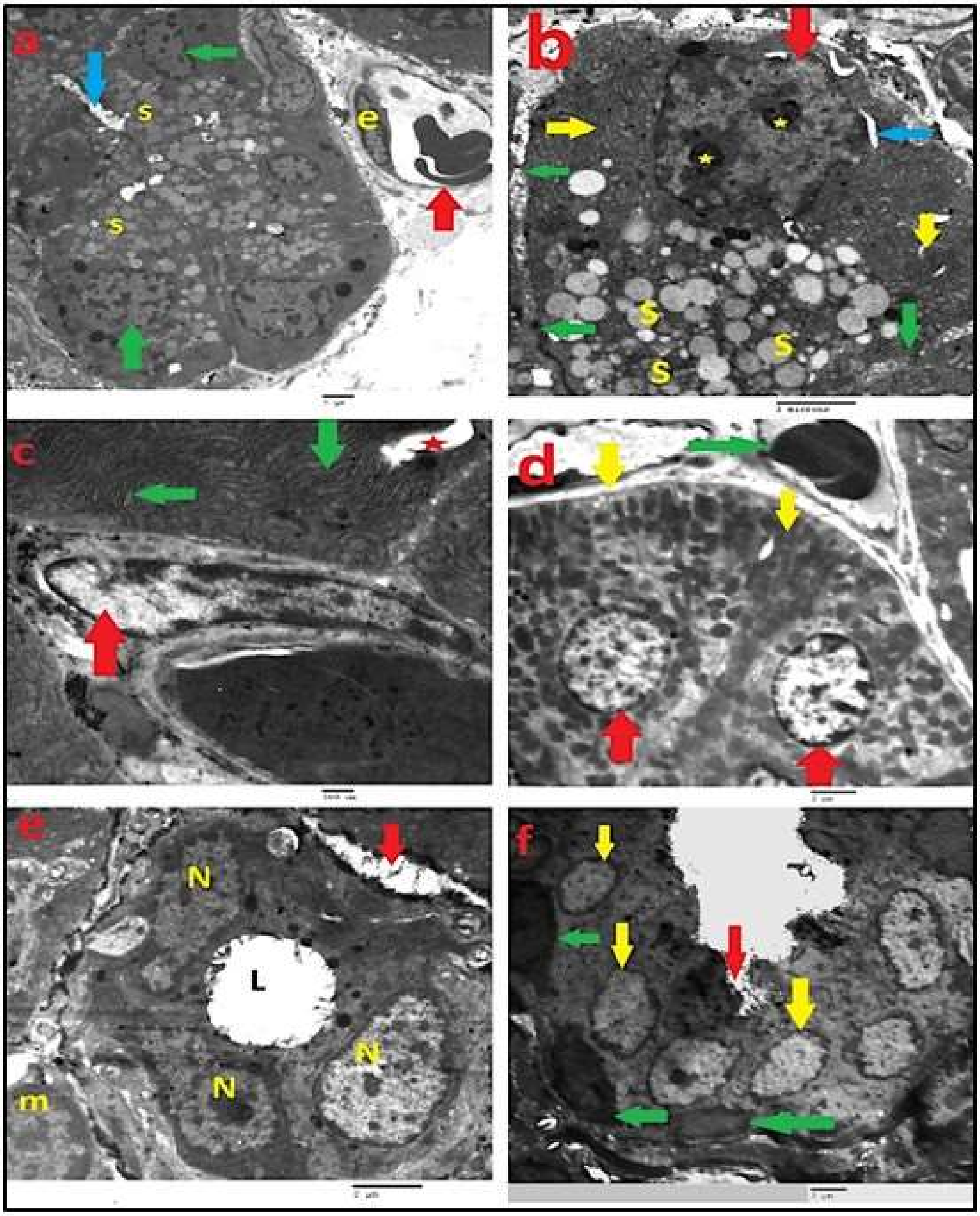

Figure 4: Electron micrograph of MSG+QN group showing: **(a)** Serous acinus with regular outline and narrow lumen (blue arrow) and pyramidal cells with basal round nuclei, some of which showed irregular nuclear membrane (green arrows), secretory granules were homogenous in size (s), normal-looking BV (red arrow) lined by flat endothelial cell (e). **(b)** Acinar cell with pyramidal outline & incomplete restoration of junctional complex (green arrows), basal round nucleus with irregular membrane (red arrow) and two prominent nucleoli (star), surrounded by parallel arrays or RER (yellow arrows), relatively less cytoplasmic vacuoles (blue arrow), homogenous apical secretory granules (s). **(c)** Basal part of acinar cell with parallel arrays of RER (green arrows), note the cytoplasmic vacuole (star), flat endothelial cell lining BV (red arrow), **(d)** SD lined by columnar cells with central round open faced nuclei with regular nuclear membrane (red arrows), relatively less swollen mitochondria & basal infoldings (yellow arrows), normal sized BV (green arrow), **(e)** ID lined by large well-arranged cuboidal cells with large nuclei occupying most of the cells (N), regular lumen (L), myoepithelial cell (m), intercellular edema (red arrow), **(f)** ED lined by pseudostratified epithelium basal cells (green arrows) & columnar cells (yellow arrows), microvilli extended into the lumen (red arrows), **[Uranyl acetate and lead citrate (a)x1000, (b)x10000, (c)x4000, (d)x1500, (e)x2000, (f)x1200].**

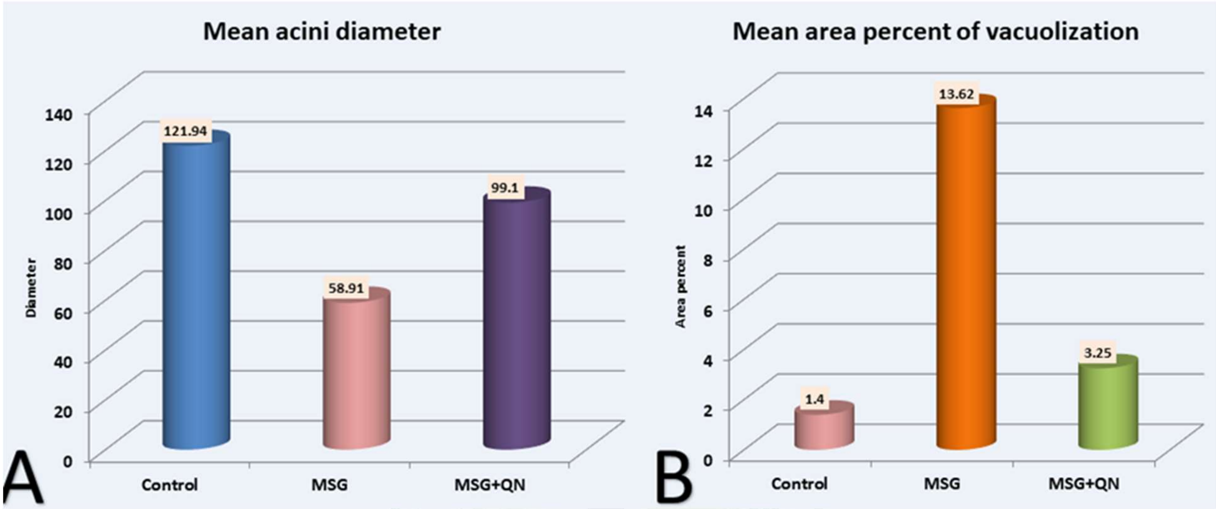

Figure 5: Bar charts for morphometric analysis. A: Column chart showing mean acinar diameter in all groups. B: Column chart showing mean area percent of vacuolization in all groups.

Discussion

In this study the Parotid gland tissue damage by MSG and the possible healing effect of QN were investigated on a histologic and ultrastructural levels. Parotid glands of the MSG group revealed serous acini with disturbed architecture and irregular margins, acinar shrinkage, and some of them were degenerated. This finding correlated to a study done by Litvak et al. in which rats developed changes in the exocrine and endocrine lobes of the pancreas due to atrophy, degeneration, and inflammation secondary to MSG administration.[20]

Regarding cytoplasmic vacuolation, the same results were reported by Sahin et al. in hepatocytes of rats. It showed that in the MSG group, vacuolated hepatocytes and cellular degeneration were observed according to the histologic and immunohistochemical findings indicating an increase in ROS load.[21] This can be illustrated by the role that MSG plays, which raises the intracellular (ROS) levels, triggering protein ubiquitination and unfolded protein response (UPR), leading to Ca2+ discharge from the endoplasmic reticulum (ER) via inositol trisphosphate receptor (IP3R)-operated stores, and finally cytoplasmic vacuolation and cell death.[22] The cytoplasmic vacuolation caused by comulative effect of ROS was also presented in a study done by Abelmeguid et al. that investigated the oxidative stress caused by Tartrazine on PG of rats.[23]

Our findings were also consistent with those of other investigations. Variations in sizes, pleomorphism, and pyknosis in nuclei of hepatocytes of MSG-treated animals,[24] also same observations were found in MSG treated gingival tissues.[25]

Some giant nuclei were detected in acinar cells of MSG group, enlargement of nucleus and giant cell might be due to inability of cell to divide although continued synthesis of certain constituents of cell.[26]

The inflammatory cell infiltration that we found can be explained by the fact that

MSG enhances levels of inflammatory mediators, especially interleukin-6 and TNFα, resulting in more recruitment of inflammatory cells [6].

Dilated and congested BVs were clearly noticed, which is consistent with many studies that found vascular congestion in the sinusoids of liver tissues,[27] along with leukocyte infiltration and increased connective tissue in the portal triads.[21] A rational explanation for this is the destructive action of ROS on endothelial cells and the architecture of the vessel wall.

Regarding ultrastructural effects, oxidative stress has been the subject of numerous studies, and it is now widely recognized as one of the mechanisms by which MSG exerts its toxic effects. Our findings came in agreement with El Imam & Abd El Salam where inspection of Submandibular gland (SMG) subjected to MSG illustrated changes such as abnormal nuclei characterized by heterochromatin clumping and margination, wide perinuclear membrane, degraded mitochondria, inflated RER cisternae, dilated intracellular canaliculi, and poorly outlined secretory granules. These apoptotic features, which also include intracellular vacuolations, cell shrinkage, changes in cell membrane are due to lipid peroxidation. ROS damages the cellular membranes and reduces the cellular ATP leading to diminished energy essential for cellular functions resulting in apoptosis.[28]

Also our findings agreed with Zhou et al. who studied the ultrastructural effects of oxidative stress on rats liver and found that the hepatocytes displayed fuzzy nuclear and mitochondrial membranes, distended ER and exacerbated vacuolar degeneration.[29] Meanwhile, Lee et al. explained that mitochondrial damage occurs when there is an accumulation of mitochondrial DNA abnormalities due to the production of ROS production and atypical mtDNA repair. This leads to discrepancies in mitochondrial respiration and ATP production. The increased ROS levels also result in excessive oxidative stress, which can further contribute to an escalating amount of unfolded or misfolded proteins in the mitochondrial matrix.[30] Moreover, Tse et al. found that increased oxidative stress has been linked to aberrant function of intracellular organelles, such as the ER and mitochondria.[31]

Interstitial edema observed in our study came in parallel with Mukherjee et al. who reported that MSG exposure increased the levels of Matrix Metalloproteinases (MMPs), which in turn increased the invasiveness of trophoblasts in placental tissues by degrading the extracellular matrix.[32]

It was found that the magnitude of effects appeared due to administration of MSG is dose dependent,[14,24,28,33–35] so, it is prudent to research not only the recognized toxic levels of MSG, but also the impact (on a living organism) of molecular mechanisms of the "safe" approved doses of MSG.

Quercetin was selected in this study to test its potency for alleviating the histological and ultrastructural alterations in parotid glands exposed to MSG. This choice was based on its extensive use as an antioxidant in numerous investigations on various tissues in which it exhibits a significant antioxidant action by sustaining an oxidative balanced environment.[10]

Our findings are consistent with earlier research that found an increased impact of QN on various tissues that are harmed by MSG or other damaging stimuli with similar destructive mechanisms.

PG tissues of rats given QN together with MSG exhibited less distortion of the acinar and ductal outline, as well as less cellular shrinkage and degeneration, compared to those given only MSG. This finding is consistent with the study conducted by Mirzakhni et al. which showed that renal tissues treated with QN (10. 00 mg/kg) together with MSG had reduced congestion and glomerular shrinkage.[15]

Also, we noticed a significant decrease in cytoplasmic vacuolations and inflammatory cell infiltration, as Firgani & Sarhan found in neuroglia and motor neurons of rats that received MSG.[13]

Additionally, it was noticed that in liver tissues of rats administered QN (10 mg/kg BW) there were less intracellular vacuolation of hepatocytes and inflammatory cell infiltration in the portal space.[11]

Akang et al. combined QN with another antioxidant (naringenin), and their synergism considerably enhanced the deteriorated antioxidant enzymatic level (triggered by antiretroviral drug activity used in this study). Furthermore, it improved the distorted hepatic cytoarchitecture.[36] This improvement might be attributed to the antioxidants' capacity to limit the activity of ROS-forming enzymes such as NADPH-oxidase and myeloperoxidase, while also increasing ROS scavengers through their capacity to create adequate hydroxyl (-OH) substitute [37].

Meanwhile, there were less but still present nuclear pleomorphism and hyperchromatism in MSG+QN group. However, in a study done which evaluated the protective effect of QN on rats' submandibular glands subjected to ZnO toxicity, QN here was used in a dose of 200 mg/kg BW and showed acinar and ductal nuclei more similar to the control group, which showed that QN enhancing effects increased with increasing its dose.[38]

Since QN has poor water solubility and low bioavailability (10%),[39] several studies have been conducted to change its structure in order to boost its water solubility and bioavailability, hence increasing its antioxidant effect. It was discovered that the integration of conjugates improves the bioavailability of free quercetin, hence increasing its antioxidant action.[10] Therefore, we recommend further studies to clarify the therapeutic potential of quercetin complexes, as well as their applications.

Conclusion

Administration of QN has protective effects on parotid gland damage induced by chronic intake of MSG. Nonetheless, the observed results provide an encouraging foundation for modulating future formulations on a variety of dosages to get the optimal dose.

Funding

This research received no specific grant from any funding agency in the public, commercial, or not-for-profit sectors.

Data availability

The datasets generated and/or analyzed during the current study are available from the corresponding author on reasonable request.

Ethical approval and consent to participate

The experiment was conducted according to the "Guide for the Care and Use of Laboratory Animals" 8th ed., 2011, The Research Ethics Committee of the Faculty of Dentistry at Ain Shams University gave their approval for the experimental design (Approval number: FDASU-Rec IM122111).

Competing interests

The authors assert explicitly that they have no known competing financial concerns or personal relationships with third parties that could appear to have influenced the effort disclosed in this study.

References

1. Chakraborty SP. Patho-physiological and toxicological aspects of monosodium glutamate. *Toxicol Mech Methods*. 2019;29(6):389-396. doi:10.1080/15376516.2018.1528649
2. Kazmi Z, Fatima I, Perveen S, Malik SS. Monosodium glutamate: Review on clinical reports. *Int J Food Prop*. 2017;20(sup2):1807-1815. doi:10.1080/10942912.2017.1295260
3. Zanfirescu A, Ungurianu A, Tsatsakis AM, et al. A Review of the Alleged Health Hazards of

Monosodium Glutamate. *Compr Rev Food Sci Food Saf*. 2019;18(4):1111-1134. doi:10.1111/1541-4337.12448
4. Yachmin A, Yeroshenko G, Shevchenko K, Perederii N, Ryabushko O. MONOSODIUM GLUTAMATE (E621) AND ITS EFFECT ON THE GASTROINTESTINAL ORGANS (REVIEW). *Georgian Med News*. 2021;(319):147-151.
5. Singh K, Sharma J, Kaur A, Ahluwalia P. Alteration upon Oral Ingestion of Monosodium Glutamate in Various Lipid and Lipoprotein Fractions in Serum of Adult Male Rat. *J Life Sci*. 2011;3(1):17-21. doi:10.1080/09751270.2011.11885164
6. Roman-Ramos R, Almanza-Perez JC, Garcia-Macedo R, et al. Monosodium glutamate neonatal intoxication associated with obesity in adult stage is characterized by chronic inflammation and increased mRNA expression of peroxisome proliferator-activated receptors in mice. *Basic Clin Pharmacol Toxicol*. 2011;108(6):406-413. doi:10.1111/j.1742-7843.2011.00671.x
7. Anand David AV, Arulmoli R, Parasuraman S. Overviews of Biological Importance of Quercetin: A Bioactive Flavonoid. *Pharmacogn Rev*. 2016;10(20):84-89. doi:10.4103/0973-7847.194044
8. Zhang M, Swarts SG, Yin L, et al. Antioxidant Properties of Quercetin. In: LaManna JC, Puchowicz MA, Xu K, Harrison DK, Bruley DF, eds. *Oxygen Transport to Tissue XXXII*. Advances in Experimental Medicine and Biology. Springer US; 2011:283-289. doi:10.1007/978-1-4419-7756-4_38
9. Oboh G, Ademosun AO, Ogunsuyi OB. Quercetin and Its Role in Chronic Diseases. In: Gupta SC, Prasad S, Aggarwal BB, eds. *Drug Discovery from Mother Nature*. Advances in Experimental Medicine and Biology. Springer International Publishing; 2016:377-387. doi:10.1007/978-3-319-41342-6_17
10. Xu D, Hu MJ, Wang YQ, Cui YL. Antioxidant Activities of Quercetin and Its Complexes for Medicinal Application. *Mol Basel Switz*. 2019;24(6):1123. doi:10.3390/molecules24061123
11. Gholampour F, Saki N. Hepatic and renal protective effects of quercetin in ferrous sulfateinduced toxicity. *Gen Physiol Biophys*. 2019;38(1):27-38. doi:10.4149/gpb_2018038
12. Gorbenko NI, Borikov OY, Kiprych TV, Ivanova OV, Taran KV, Litvinova TS. Quercetin improves myocardial redox status in rats with type 2 diabetes. *Endocr Regul*. 2021;55(3):142-152. doi:10.2478/enr-2021-0015
13. Firgany AEDL, Sarhan NR. Quercetin mitigates monosodium glutamate-induced excitotoxicity of the spinal cord motoneurons in aged rats via p38 MAPK inhibition. *Acta Histochem*. 2020;122(5):151554. doi:10.1016/j.acthis.2020.151554
14. Moubarak H. HISTOLOGICAL AND IMMUNOHISTOCHEMICAL EVALUATION OF THE EFFECT OF MONOSODIUM GLUTAMATE ON PAROTID SALIVARY GLANDS OF ADULT MALE ALBINO RATS. *Egypt Dent J*. 2015;61:4557:4565.
15. Mirzakhani N, Farshid AA, Tehrani AA, Tamaddonfard E, Imani M. Comparison of the effects of hydroalcoholic extract of Capparis spinosa fruit, quercetin and vitamin E on monosodium glutamate-induced toxicity in rats. *Vet Res Forum*. 2020;11(2). doi:10.30466/vrf.2018.83041.2091
16. Sotnikova R, Nosalova V, Navarova J. Efficacy of quercetin derivatives in prevention of ulcerative colitis in rats. *Interdiscip Toxicol*. 2013;6(1):9-12. doi:10.2478/intox-2013-0002
17. Bindhu P, Krishnapillai R, Thomas P, Jayanthi P. Facts in artifacts. *J Oral Maxillofac Pathol*. 2013;17(3):397. doi:10.4103/0973-029X.125206
18. Morsy MB, Abd ElHameed MM, Fathy IA. The Possible Modulatory Effect of Vitamin E Administration on Submandibular Salivary Gland of Albino Rats receiving Fat Rich Diet: A histological and ultrastructural study. *Egypt J Histol*. 2023;0. doi:10.21608/ejh.2023.188090.1844
19. Hayat MA. *Principals and Techniques of Electron Microscopy: Biological Applications. 4th ED. Cambridge University Press, Edinburgh, UK.* 4th ed.; 2000.
20. Litvak YV, Harapko T, Lytvak V, Foros AI. MORPHOLOGICAL PECULIARITIES OF THE PANCREAS OF MALE RATS AFTER PROLONGED ADMINISTRATION OF MONOSODIUM GLUTAMATE DURING THE RECOVERY PERIOD. *Wiadomosci Lek Wars Pol 1960*. 2022;75(12):3102-3108. doi:10.36740/WLek202212135
21. Sahin B, Acikel Elmas M, Bingol Ozakpinar O, Arbak S. The Effects of Apocynin on Monosodium Glutamate Induced Liver Damage of Rats. *Heliyon*. 2023;9(7):e17327. doi:10.1016/j.heliyon.2023.e17327
22. Zheng K, Liao C, Li Y, et al. Gypenoside L, Isolated from Gynostemma pentaphyllum, Induces Cytoplasmic Vacuolation Death in Hepatocellular Carcinoma Cells through Reactive-Oxygen-Species-Mediated Unfolded Protein Response. *J Agric Food Chem*. 2016;64(8):1702-1711. doi:10.1021/acs.jafc.5b05668
23. Abelmeguid IM, Elsharkawy RT, Obeid RF. Histopathological evaluation of the effect of vitamin E on reversing changes induced by Tartrazine in parotid glands of albino rats. *Ain Shams Dent J*. 2022;25(1):84-91. doi:10.21608/asdj.2022.158424.1137

24. Onaolapo O, Onaolapo A, Mosaku T, Onigbinde O, Abiodun O. *A Histological Study of the Hepatic and Renal Effects of Subchronic Low Dose Oral Monosodium Glutamate in Swiss Albino Mice*.; 2013. doi:10.13140/RG.2.2.33979.23848
25. Shredah MT. Molecular study to the effect of monosodium glutamate on rat gingiva. *Tanta Dent J*. 2017;14(3):155. doi:10.4103/tdj.tdj_21_17
26. Fendrick SE, Xue QS, Streit WJ. Formation of multinucleated giant cells and microglial degeneration in rats expressing a mutant Cu/Zn superoxide dismutase gene. *J Neuroinflammation*. 2007;4(1):9. doi:10.1186/1742-2094-4-9
27. EL-Meghawry EL-Kenawy A, Osman HEH, Daghestani MH. The effect of vitamin C administration on monosodium glutamate induced liver injury. An experimental study. *Exp Toxicol Pathol*. 2013;65(5):513-521. doi:10.1016/j.etp.2012.02.007
28. El Imam H, Abd El Salam N. Histological and Ultra structural Study of the Effect of Monosodium Glutamate on the Submandibular Salivary Gland of Adult Albino Rats. *Egypt Dent J*. 2019;65(1):319-329. doi:10.21608/edj.2015.71419
29. Zhou B hua, Zhao J, Liu J, Zhang J liang, Li J, Wang H wei. Fluoride-induced oxidative stress is involved in the morphological damage and dysfunction of liver in female mice. *Chemosphere*. 2015;139:504-511. doi:10.1016/j.chemosphere.2015.08.030
30. Lee HY, Nga HT, Tian J, Yi HS. Mitochondrial Metabolic Signatures in Hepatocellular Carcinoma. *Cells*. 2021;10(8):1901. doi:10.3390/cells10081901
31. Tse G, Yan BP, Chan YWF, Tian XY, Huang Y. Reactive Oxygen Species, Endoplasmic Reticulum Stress and Mitochondrial Dysfunction: The Link with Cardiac Arrhythmogenesis. *Front Physiol*. 2016;7. Accessed September 6, 2023. https://www.frontiersin.org/articles/10.3389/fphys.2016.00313
32. Mukherjee I, Biswas S, Singh S, et al. Monosodium Glutamate Perturbs Human Trophoblast Invasion and Differentiation through a Reactive Oxygen Species-Mediated Pathway: An In-Vitro Assessment. *Antioxidants*. 2023;12(3):634. doi:10.3390/antiox12030634
33. Khalaf HA, Arafat EA. Effect of different doses of monosodium glutamate on the thyroid follicular cells of adult male albino rats: a histological study. *Int J Clin Exp Pathol*. 2015;8(12):15498-15510.
34. Delibashvili D, Dumbadze Z, Krynytska I, Marushchak M, Habor H, Holovatiuk L. THE INFLUENCE OF MONOSODIUM GLUTAMATE ADMINISTRATION ON GENERATION OF REACTIVE OXYGEN SPECIES AND APOPTOSIS OF BLOOD LEUKOCYTES IN RATS. *Georgian Med News*. 2018;(283):144-148.
35. Airaodion A, Ngwogu K, Ngwogu A, Megwas A, Ekenjoku J. Nephrotoxicity of Monosodium Glutamate (MSG) in Wistar Rats. Published online May 1, 2020:1-10.
36. Akang EN, Dosumu OO, Okoko I ibehe E, Faniyan O, Oremosu AA, Akanmu AS. Microscopic and biochemical changes on liver and kidney of Wistar rats on combination antiretroviral therapy: the impact of naringenin and quercetin. *Toxicol Res*. 2020;9(5):601-608. doi:10.1093/toxres/tfaa060
37. M M. Antioxidants: Balancing the Good, the Bad and the Ugly. *Nutr Food Technol Open Access*. 2016;2(2). doi:10.16966/2470-6086.123
38. Hamza SA. HISTOLOGICAL EVALUATION OF THE ROLE OF ZINC OXIDE NANOPARTICLES ON SUBMANDIBULAR SALIVARY GLANDS IN RATS AND THE PROPHYLACTIC EFFECT OF QUERCETIN. *Egypt Dent J*. 2019;65(Issue 2-April (Oral Medicine, X-Ray, Oral Biology&Oral Pathology)):1359-1366. doi:10.21608/edj.2019.72560
39. Kandemir K, Tomas M, McClements DJ, Capanoglu E. Recent advances on the improvement of quercetin bioavailability. *Trends Food Sci Technol*. 2022;119:192-200. doi:10.1016/j.tifs.2021.11.032